Journal of the European Ceramic Society 43 (2023) 47–53

Contents lists available at ScienceDirect

Journal of the European Ceramic Society

journal homepage: www.elsevier.com/locate/jeurceramsoc

Liquid metal infiltration of silicon based alloys into porous carbonaceous materials Part-III: Experimental verification of conversion products and infiltration depth by infiltration of Si-Zr alloy into mixed SiC/ graphite preforms

Manoj Naikade [a,b], Caroline Hain [a], Kaja Kastelik [a], Annapaola Parrilli [a], Thomas Graule [a], Ludger Weber [b], Alberto Ortona [c,*]

[a] Empa – Swiss Federal Laboratories for Materials Science and Technology, Dübendorf, Switzerland
[b] Laboratory of Mechanical Metallurgy, Ecole Polytechnique Federale de Lausanne, EPFL, Lausanne, Switzerland
[c] Scuola universitaria professionale della Svizzera italiana, Lugano, Switzerland

ARTICLE INFO

Keywords:
LSI
RMI
SiC composites
Si-Zr alloy infiltration

ABSTRACT

Porous carbonaceous preforms, made from graphite and silicon carbide (SiC) powders, with varying graphite powder mass fractions and particle sizes, were infiltrated at 1500 °C and 1700 °C by Si-8 at. pct Zr alloy to produce dense Si-Zr-SiC composites. The experiments were performed in a graphite chamber vacuum furnace at 10^{-2} mbar. The most desirable results were obtained for preforms composed of a mixture of graphite and SiC powders, with preforms containing 15–20 % mass fraction of graphite and infiltrated at 1500 °C. The banding of the Zr-rich phase observed in the cross-sections of SiC-C pre- forms infiltrated by the Si-Zr alloy may help in decoding the reactive infiltration process with binary alloys.

1. Introduction

Silicon carbide (SiC) is one of the most important and industrially applied non-oxide ceramic materials for high temperature applications, due to its exceptional thermo-mechanical strength and chemical stability. Its properties, however, can vary greatly depending on the used manufacturing method. The most common methods for obtaining dense silicon carbide are: pressureless sintering in solid state (SSiC), infiltration of reaction bonded silicon carbide by molten silicon (SiSiC), liquid phase sintered silicon carbide (LPSiC) and hot pressing (HPSiC). Silicon infiltrated silicon carbide (SiSiC), first developed by Popper in 1960s [1], is a well known industrial ceramic material due to its remarkable properties, such as low porosity, low density, high thermal conductivity, high mechanical strength, excellent chemical, oxidation and thermal shock resistance and high wear and corrosion resistance [2]. Additionally, it represents a cost-effective method to manufacture large and complex parts. SiSiC, also known as liquid silicon infiltration (LSI), involves infiltrating a porous carbonaceous preform by molten Si, which exothermically reacts with C to form SiC, resulting ideally in a dense composite. Over the past decades, Si–SiC ceramics have generated tremendous interest, which has led to the development of many variations of these materials, monolithic and particle/fibre reinforced CMCs, which can be obtained from different constituents and processes [3–8]. However, LSI has its disadvantages, the foremost being the presence of residual Si, rendering the composite unusable at temperatures near or above the melting point of Si.

Messner et al. [9] have shown that Si-alloy infiltration can be used to overcome the limitation of residual Si by replacing the residual Si with refractory silicides, characterised by higher melting temperatures. The alloying element is selected in such a way, that when Si from the alloy reacts with C to form SiC, the concentration of the alloying element increases and results in the formation of a refractory silicide. Several researchers have studied the process and properties of the Si-alloy infiltration with alloying elements, like Mo, Ti, Y, Zr, Ir, Fe, Co and Hf to produce dense SiC composites [10–19].

Reactive infiltration of porous carbonaceous preforms with Si or Si alloys is a complex process and it is affected by various parameters, e.g., pore volume fraction, pore size, shape and distribution, the reactivity of carbon depending on the type of carbonaceous phase used, as well as the particle size and shape. The preforms are usually made from a mixture of

* Correspondence to: Laboratory, MEMTi, DTI, SUPSI Polo universitario Lugano - Campus Est, Via la Santa 1 CH-6962 Lugano – Viganello.
E-mail address: alberto.ortona@supsi.ch (A. Ortona).

https://doi.org/10.1016/j.jeurceramsoc.2022.09.036
Received 6 August 2022; Received in revised form 19 September 2022; Accepted 20 September 2022
Available online 21 September 2022

C, SiC, organic binder and pore forming materials (e.g., starch). The mass fraction of each constituent plays an important role in the nature of the produced preforms and, consequently, in the reactive infiltration process itself. Most of the physical phenomena involved in the reactive infiltration process are temperature dependent. Additionally, the atmosphere inside the furnace can significantly affect the process, as the melting of the metal or alloy can be disrupted by oxidation [20–22].

In this study, a comprehensive experimental analysis of the effects of various key parameters involved in the reactive infiltration of C-C and SiC-C preforms by near eutectic Si-Zr alloy was performed. This paper is the third and last part on the study of liquid metal infiltration of silicon based alloys into porous carbonaceous materials. The main novelty in our approach stands in the validation procedure of the developed models [23], which went through infiltration experiments from ideal straight and curved channels [24] to the real porous preforms, with randomly tortuous channels, of this work.

2. Materials and methods

Graphite powders of grade TIMREX KS25 and TIMREX KS44 characterised by particle sizes, d_{90}, of 25 and 44 μm, respectively, were used in the experiments. TIMREX grades were sourced from Imerys Graphite & Carbon Switzerland Ltd. Silicon carbide powder of grade F800 (green) was sourced from Tracomme AG, Switzerland. A phenolic resin, Bakelite PF GA T 10 R from HEXION was used as the organic binder. Graphite foil and custom size graphite crucibles were sourced from SGL carbon, Germany and STEINEMANN CARBON AG, Switzerland, respectively. Near eutectic Si-8 at. pct Zr alloy (Chengdu Huarui Industrial Co Ltd., China) was used for the infiltration of the porous preforms.

The graphite powder, SiC powder, Bakelite (binder) were weighed and put in a desired proportion in a plastic bottle together with alumina balls. The bottle was then kept on a roller mill for approximately 12 h to obtain a homogeneous mixture. The mixture was next sieved to remove the alumina balls using a mechanical shaker (ASM 200, Siebtechnik GmbH, Germany).

The SiC-C preforms were prepared for studying the effect of graphite mass fraction by mixing SiC powder of grade F800 and graphite powder of TIMREX KS25 or TIMREX KS44 grade in varying proportion along with Bakelite as binder. The details of the powder mix for SiC-C preforms are summarised in Table 1.

2.1. Forming

Hot pressing was chosen to obtain green bodies with good mechanical strength. A uniaxial hot mounting press (Buehler SimpliMet 1000, USA) with a 40 mm die was used for hot pressing the powder mix. The typical compaction cycle included heating up to 150 °C in 5 min, holding for 2 min at 28 MPa, and cooling to room temperature in 3 min. The obtained thickness for the preforms was approx. 5 mm.

2.2. Pyrolysis

The prepared SiC-C preforms were then pyrolysed to carbonize the Bakelite (binder material). Pyrolysis was performed in an alumina tube furnace in an flowing argon. The SiC-C preforms were pyrolysed at 1000 °C by applying a heating rate of 60 °C/h from room temperature to 500 °C and of 200 °C/h up to 1000 °C holding for 15 min, followed by natural cooling.

2.3. Reactive infiltration

The reactive melt infiltration experiments were performed in a heated graphite vacuum furnace (FCT Systems, Germany) at an absolute pressure of approx. 10^{-2} mbar. The furnace was pre-heated at 60 °C/h up to 200 °C and held for 30 min. Then, with a heating rate of 520 °C/h, the infiltration temperature of 1500 °C was reached. This temperature was held for 1 h, after which the heating was turned off and the furnace was left to cool.

Fig. 1 shows the infiltration set up. To contain molten silicon 0.5 mm thick graphite foils were used to form cylinders, which were next glued using a mixture of Bakelite resin and isopropyl alcohol (50–50 wt%). Circular pieces of graphite foil were glued to the bottom of the cylinders and cured at 120 °C. Later, the cured crucibles were pyrolysed at 1000 °C to transform the resin into carbon. The inner walls of the crucibles were sprayed with BN (sourced from 3 M ™) to reduce its direct reaction with molten Si and the Si-Zr alloy.

2.4. Characterisation

The particle size distribution and the density of the graphite powders, SiC powder and their mixtures were measured using a laser diffraction particle size analyzer (LS 13320 Beckman Coulter, United States) and a helium pycnometer (AccuPyc II 1340, Micromeritics, United States), respectively. The porosity and the pore size distribution of the pyrolysed preforms were measured via mercury intrusion porosimetry (MIP) (PASCAL 140/400, Thermo Finnigan, Germany). The skeletal densities from helium pycnometry were used for porosity calculations using Hg porosimetry. X-ray tomography (RX solution Easy-Tom XL, France) was also used to analyse the porosity of the pyrolysed preforms.

The cross-sections of the infiltrated preforms were cut using a diamond saw and cold mounted in epoxy resin (SpeciFix Resin, Struers, Germany). Initially, automatic grinding of the samples was carried out using a 40 μm diamond pad, followed by automatic polishing performed using 6, 3 and 1 μm diamond suspensions and final polishing with an acidic aluminium oxide suspension. SEM and EDX analysis of the polished samples was done using the Tescan VEGA3 scanning electron microscope with Bruker AXS Quantax 200 EDX system.

Table 1
Summary of powder mix used to make the SiC-C preforms to determine the effect of mass fraction of graphite and SiC powder.

Mix name	SiC F800	TIMREX KS25	TIMREX KS44	Bakelite
	wt%	wt%	wt%	wt%
SiC C 01	90	0		10
SiC C 02	85	5		10
SiC C 03	80	10		10
SiC C 04	75	15		10
SiC C 05	70	20		10
SiC C 06	65	25		10
SiC C 07	60	30		10
SiC C 08	70		20	10
SiC C 09	65		25	10
SiC C 10	60		30	10

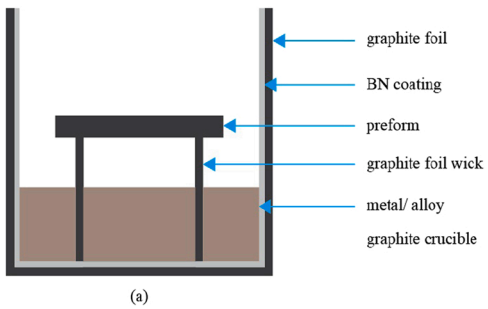

Fig. 1. Schematic of preform infiltration setup using graphite foil crucible having inner walls coated with BN.

3. Results

The graphite powder particles are flaky in shape, while the SiC F800 powder particles are angular, as can be seen in the SEM images in Fig. 2.

The median diameter and percentage porosity of both, TIMREX KS25 and TIMREX KS44 containing preforms, changed with increasing graphite fraction (Fig. 3). The median pore diameter was in the range of 1.6–3.4 μm, and preform porosity ranged from 30 % to 44 %, with both preforms found to decrease with increasing graphite powder fraction. Porosity as well as particles sizes and shape were accurately measured. Further details can be found in the Supplementary material.

3.1. Infiltration of SiC-C preforms with near eutectic Si-Zr alloy

SEM cross-section images of SiC-C preforms fabricated with varying TIMREX KS25 graphite mass fractions from 5 % to 30 %, infiltrated by the near- eutectic Si-Zr alloy at 1500 °C, are shown in Fig. 4. Complete infiltration was achieved along the thickness of the preforms, except for the sample with 30 % graphite powder, where the centre is not reached by the liquid alloy. For samples with 5 % and 10 % graphite powder, banding of the Zr-rich phase can be seen. It decreases with increasing graphite content until reaching 20 %. The sample with 25 % graphite powder shows a single band at the centre with a Zr-rich phase, while the sample with 30 % graphite shows 2 bands of a Zr-rich phase close to the centre and an uninfiltrated centre with a thickness of slightly less than 1/3 of the total thickness. Porosity can be observed at the centre of the samples with 5% and 10% graphite powder, the latter being more porous. The samples with 15 % and 20 % graphite powder show the most uniform structure considering the distribution of the Zr-rich phase, as well as exhibiting minimal porosity.

The SEM cross-section images of the samples made from 20 %, 25 % and 30 % TIMREX KS25 graphite powder and infiltrated by the near-eutectic Si-Zr alloy at 1700 °C, are shown in Fig. 5. Only the sample with 20 % graphite was completely infiltrated by the alloy, whereas samples with 25 % and 30 % graphite have approximately 1/3 and 3/4 of the total thickness at the core not infiltrated by the alloy. The sample with 20 % of graphite powder shows a single band of Zr-rich phase at the centre, where uninfiltrated pores can also be observed. The samples with 25 % and 30 % graphite powder are characterised by Zr-rich phase bands located just before the alloy stops. Furthermore, these samples possess high porosity in the infiltrated zones.

In Fig. 6, the SEM cross-section images are shown of the preforms fabricated using the TIMREX KS44 graphite powder with mass fractions of 20 %, 25 % and 30 % and infiltrated by the near-eutectic Si-Zr alloy at 1500 °C. The preforms with 20 % and 25 % graphite powder were completely infiltrated by the Si-Zr alloy. Both of the samples show a fair amount of uninfiltrated porosity, which is homogeneously distributed throughout the entire thickness of the preform. The samples showed a single band at the centre with a Zr-rich phase. The molten Si-Zr alloy was not able to reach the core of the sample with 30 % graphite powder,

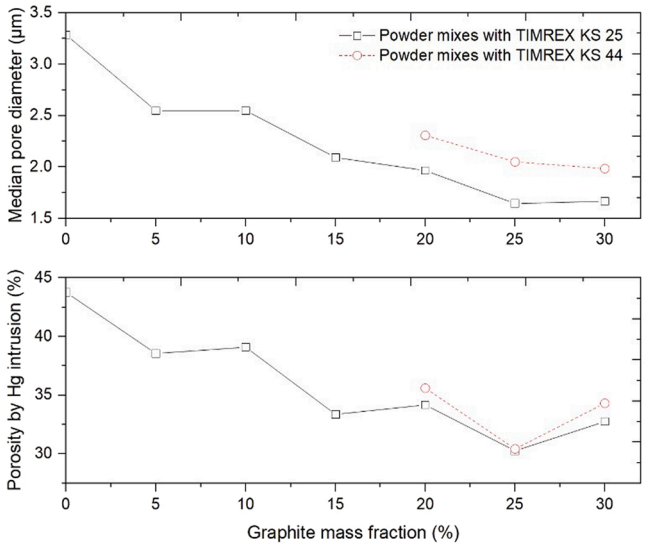

Fig. 3. Median pore size and total percentage porosity SiC-C preforms as a function of graphite fraction, measured via MIP.

where almost 1/3 of the total thickness remained uninfiltrated at the centre. Two bands with a Zr-rich phase can be observed where the alloy stops infiltrating near the centre from both top and bottom side. The infiltrated zone additionally showed a significant amount of homogeneously distributed uninfiltrated pores.

The XRD analysis of the selected area from the infiltrated preforms are shown in Fig. 7. The major phases observed are SiC, C, Si, Si_2Zr, as well as some impurity phases containing Hf, Al and Fe. For the partially infiltrated samples, only the reacted zones were chosen for analysis. The presence of peaks from Si and C in nearly all preforms, although in lower intensities, suggests the presence of residual Si and unreacted C.

4. Discussion

A successful reactive melt infiltration requires sufficient capillary forces, as they pull the melt into the open pores of the preform. Parameters, such as the contact angle between the preform material and melt, pore size, atmosphere in the furnace during infiltration, and surface tension of the infiltrating melt affect the capillary forces. Moreover, during the infiltration process, it is important that the capillary network remains open. The reactive infiltration of SiC-C preforms is a very complex process due to the competing of simultaneously occurring processes, such as the pulling of the liquid by capillary action into the pores and the conversion of C into SiC by exothermic reaction. The extent of infiltration and conversion of C to SiC is decisive for the resulting properties of the composite. Several observations were carried

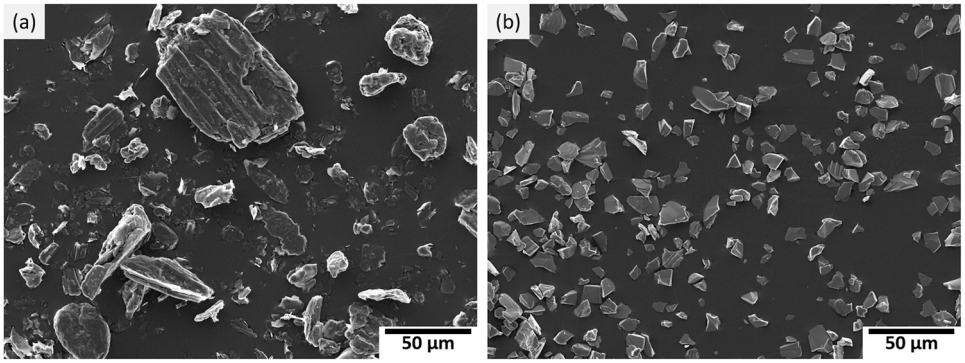

Fig. 2. SEM images of the TIMREX KS 44 graphite powder (left) and SiC F800 powder (right) showing their flaky and angular shape, respectively.

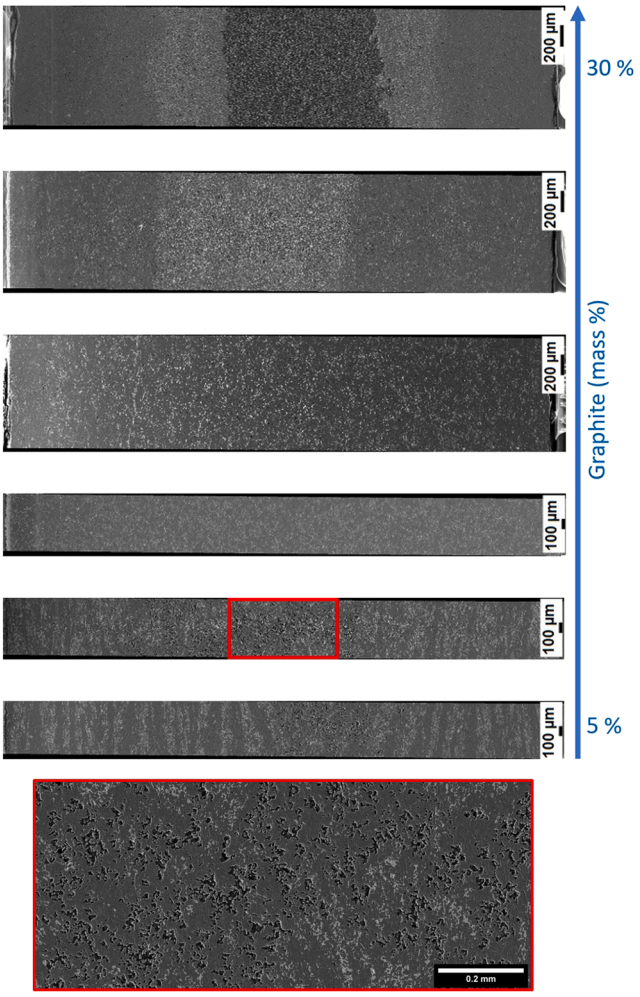

Fig. 4. Stitched HR-SEM cross-section images of SiC-C preforms with increasing mass fraction of TIMREX KS25 graphite powder from 5% to 30% and infiltrated by near eutectic Si-Zr alloy at 1500 °C. A magnified area in the red rectangle highlights the observed porosity.

out on the SiC-C preforms before and after the infiltration by the near-eutectic Si-Zr alloy. The effect of preform parameters, e.g. particle and porosity size and their distribution (see supplementary material), graphite mass fraction and infiltration temperature exhibit an explicit influence on the extent of the infiltration of the preform, as well as the conversion of the graphite powder particles to SiC.

The addition of SiC powder to the graphite powder considerably reduces the necessary initial porosity of preforms, as shown in the analytical model for adequate porosity, in our previous work [23]. This is beneficial in making green preforms with a lower porosity, and thus higher strength.

Fig. 8, depicts the plotted values of the theoretical adequate porosity to attain composites without any residual porosity or unreacted Si. This is obtained by facilitating the complete conversion of graphite along with the measured porosity values of SiC/C preforms made from SiC F800 powder and TIMREX KS 25 graphite with varying mass fraction using two different methods, namely, MIP, and CT tomography and skeletal density measured by He pycnometry. The analytical model developed in our previous work [23] is used for calculating the ideal porosity value. For the calculation and bakelite's pyrolytic carbon yield was taken as 60 %.

The infiltration results of the SiC-C preforms with varying mass fractions of graphite powder are affected not only by the amount of graphite available for the reaction with the alloy but also the changing porosity distribution of the preforms. It is evident from the porosity analysis of the preforms that the porosity decreases with the increasing mass fraction of graphite powder in the preform. The equivalent radius R^* for the SiC/C preforms is calculated using the derivation developed in our previous work [23]. The factor φ, accounting for the influence of the SiC particles in wetting, is also calculated by taking the ratio of the surface provided by the graphite to the surface per volume of graphite and SiC together are given in Table 2.

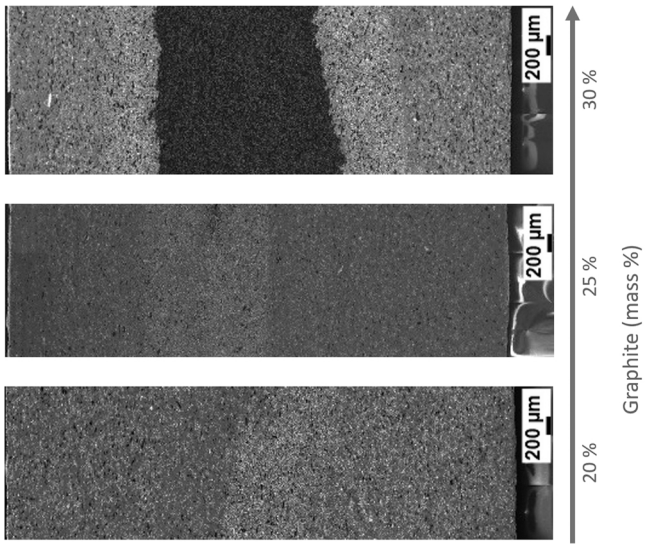

Fig. 6. The high resolution SEM images stitched to together to make panorama of the cross-section of the SiC-C preforms with increasing mass fraction of TIMREX KS44 graphite powder from 20% to 30% and infiltrated by near eutectic Si-Zr alloy at 1500 °C.

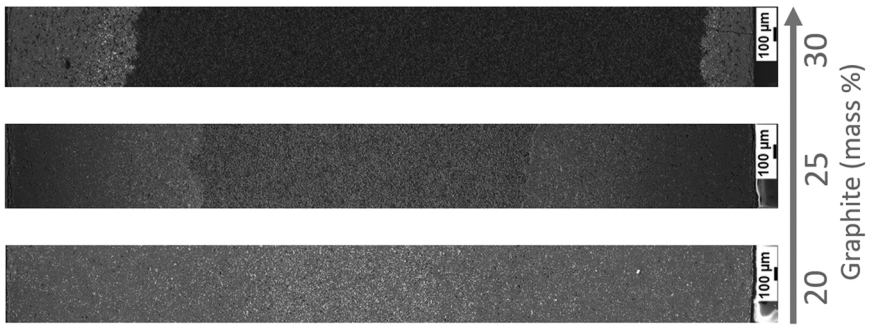

Fig. 5. Stitched HR-SEM cross-section images of SiC-C preforms with increasing mass fraction of TIMREX KS25 graphite powder from 20% to 30% and infiltrated by near eutectic Si-Zr alloy at 1700 °C.

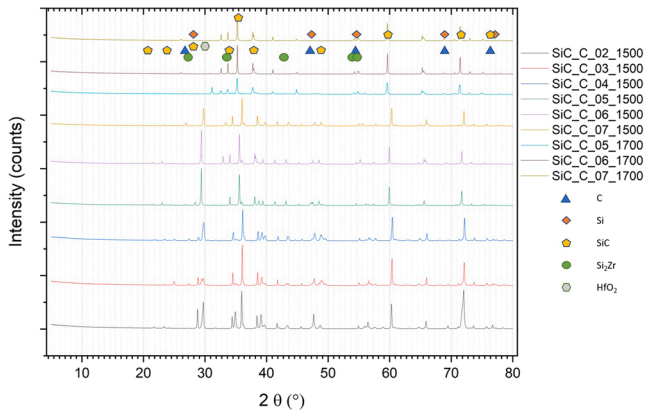

Fig. 7. XRD analysis of SiC/C preforms after infiltration at 1500 °C and 1700 °C show- ing major phases observed, which were C, Si, SI2Zr and some unidentified impurity phases containing Hf, Al and Fe.

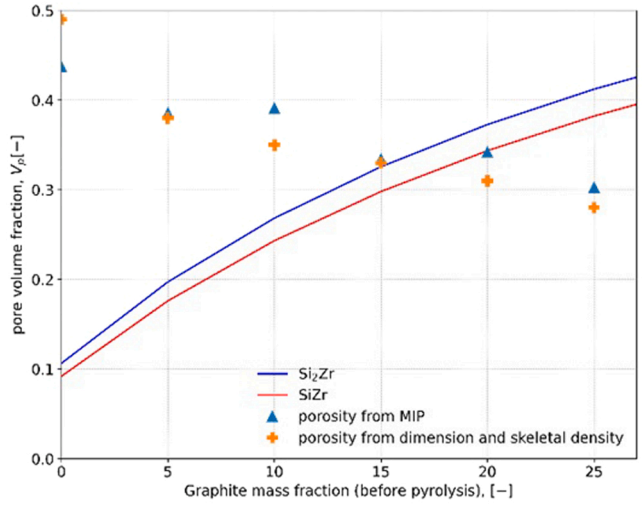

Fig. 8. Theoretical initial adequate porosity of the SiC/C preforms with varying graphite fractions to obtain fully dense preforms without residual Si or unreacted C and given silicide phase. Above the line one would expect to get free Si and below the line unreacted C. The measured porosity values are also shown for preforms with TIMREX KS 25 graphite powder mass fractions ranging from 5 % to 25 %.

The effect of pyrolysed carbon from Bakelite was not considered for simplification. The value of specific surface of SiC F800 is taken as 1,07 m^2/g from ref [25], the values for TIMREX KS25 and TIMREX KS44 are respectively 12 and 9 m^2/g.

The terminal infiltration length L, is calculated with the differential model presented in our previous work[23] (Fig. 9). It is calculated considering a non-isothermal infiltration of Si-8 at-pct Zr alloy for a temperature of 1500 °C and 1700 °C with of R^* and φ values of Table 2.

Table 2
The calculated values of equivalent radius, R* and SiC propensity factor, φ in the SiC/C preforms as developed in our previous work [23].

Sample	Graphite powder	Graphite mass fraction	R* [m]	φ
SiC C 01	TIMREX KS 25	0	5.60E-07	0
SiC C 02	TIMREX KS 25	5	2.50E-07	0.37
SiC C 03	TIMREX KS 25	10	1.60E-07	0.55
SiC C 04	TIMREX KS 25	15	1.20E-07	0.66
SiC C 05	TIMREX KS 25	20	9.30E-08	0.74
SiC C 06	TIMREX KS 25	25	7.00E-08	0.79
SiC C 07	TIMREX KS 25	30	5.60E-08	0.83
SiC C 08	TIMREX KS 44	20	1.20E-07	0.68
SiC C 09	TIMREX KS 44	25	9.50E-08	0.74
SiC C 10	TIMREX KS 44	30	7.70E-08	0.78

The infiltration lengths qualitatively follow the model when compared with the SEM micrographs in Fig. 4, Fig. 5 and Fig. 6. The measured infiltration lengths are intentionally not plotted as they do not consider the tortuosity of the pore network into the preform. The most desirable results, which include a homogeneous distribution of the Zr-rich phase, least porosity and maximum conversion of graphite into SiC, can be seen in sample with 15 % and 20 % mass fraction of graphite for preforms with both TIMREX KS25 and 20 % mass fraction of TIMREX KS44 powder. The last one, however, has approximately 4–6% of unreacted graphite. The uncertainty is due to the difficulty in the segmentation of the pores and residual graphite due to low image contrast. The porosity values are close to those calculated by the analytical model (Fig. 9).

There is another interesting observation from the preforms with TIMREX KS25 powder infiltrated at 1700 °C, as seen in Fig. 5: the preforms with 25 % and 30 % graphite show much less depth of infiltration when compared to those of the same preforms infiltrated at 1500 °C. Regarding the calculated terminal length in Fig. 9, the preforms should actually show longer infiltration depths. As also observed in our previous work [23], the increase in temperature in non-isothermal infiltration may increase the infiltration depth achieved for a given capillary size. However, in the case of the porous carbonaceous preform, the pore structure is more random and sometimes small enough to locally have a negative effect on the reactive infiltration process, as seen in the isothermal case (Fig. 10).

Again, the terminal length values are lower than that of those obtained in non-isothermal infiltration. This has to do with the fact that diffusion-mediated infiltration is possible in the incremental scheme used in the non-isothermal modelling, while in the isothermal model, the infiltration stops as soon as the defined critical concentration is attained for the first time. Nonetheless, the model requires further development, as some of the basic assumptions do no longer hold when calculating short infiltrations at diffusion-mediated "creeping" infiltration rates.

4.1. Banding of the Zr-rich phase

The banding of the Zr-rich phase observed in the cross-sections of SiC-C pre- forms infiltrated by the Si-Zr alloy may help in decoding the reactive infiltration process with binary alloys. In our previous work [24], where we studied the reactive flow of molten pure Si and Si-Zr alloy in a single micron-size capillary channel machined into glassy carbon, we found two distinct mechanisms, which could cause the

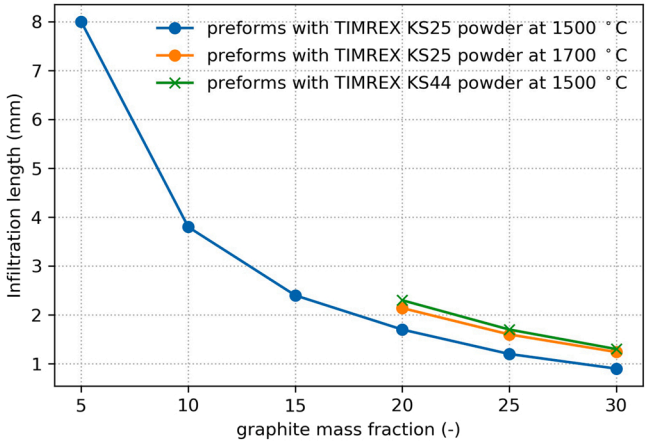

Fig. 9. The calculated terminal infiltration length of the SiC/C preforms for a non- isothermal case, inputting the graphite mass fraction and infiltration temperature values used in this study.

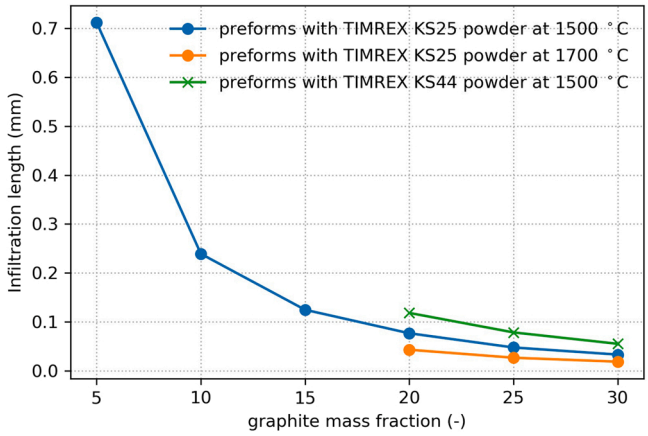

Fig. 10. The calculated terminal infiltration length for an isothermal infiltration case. The temperature has a negative effect on the terminal infiltration depth.

infiltration to stop during the reactive infiltration of molten Si-Zr alloy. The first is the widely suggested formation of solid SiC due to the reaction between carbon and molten silicon reducing the permeability of the channels until it blocks the further supply of fresh molten Si or alloy from the ingress to complete the infiltration of the preform. The second mechanism we found is the precipitation of solid zirconium silicides at the infiltration front due to the increase in Zr concentration in the alloy along the infiltration path as Si reacts with carbon to form SiC. These combined findings of the analytical model for ideal porosity and infiltration length suggests that as the graphite fraction increases the infiltration depth should also increase for a given porosity.

In Fig. 4, the SEM cross-section image of the preform with 5% TIMREX KS25 graphite powder infiltrated at 1500 °C shows an alternating band structure of a Zr-rich phase and reaction-formed SiC along the length with a large amount of residual porosity at the core. Since the SEM image depicts only a small width (few 100 μm) compared to the whole thickness of the preform (~5 mm), it might give an impression of ordered banding of the Zr-rich phase. The lower magnification image (Fig. 11), however, shows typical off-eutectic solidification. As the amount of C in the preform is much lower, the composition infiltrated alloy after reaction with C changes slightly and results in the observed off- eutectic solidification.

The preforms with 15 % and 20 % TIMREX KS25 graphite powder infiltrated at 1500 °C are characterised by a homogeneous distribution of Zr silicides without any banding and the least residual porosity as measured by grayscale thresholding of high resolution panoramic SEM images of the cross-sections in Fig. 4. The measured densities after infiltration for preforms with 15 % and 20 % graphite powder are 3.39 g/cm^3 and 3.34 g/cm^3, respectively. The homogeneous structure suggests that the preforms are infiltrated fast enough to avoid pore closure caused by Zr silicide precipitation, resulting in a homogeneous precipitation of Zr silicides after the Si from the alloy has reacted with the graphite particles to form SiC and, consequently, increasing the Zr concentration in the remaining liquid. When the concentration of graphite mass fraction is increased to 25 %, a single band with a high concentration of a Zr-rich phase can be seen at the core with slight residual porosity. Therefore, the density after infiltration is slightly lower than that of the preform with a graphite mass fraction of 20 %. The increase in graphite mass fraction in the preform with 25 % graphite powder increases the Zr concentration at the infiltration front more than that of preform with graphite mass fraction of 20 %, as there is more C available to react with Si. When the graphite mass fraction is further increased to 30 %, the initial preform porosity value decreases considerably, compared to the ideal porosity and the amount of graphite to react with the Si from the alloy is high enough to increase the concentration of Zr at the infiltration front at a much shorter length, such that the precipitation of Zr silicides blocks further supplies of fresh alloy to the core of the preform. This can be seen as the two bright colour bands of Zr-rich phase on both sides of the uninfiltrated preform core of the SEM micrographs.

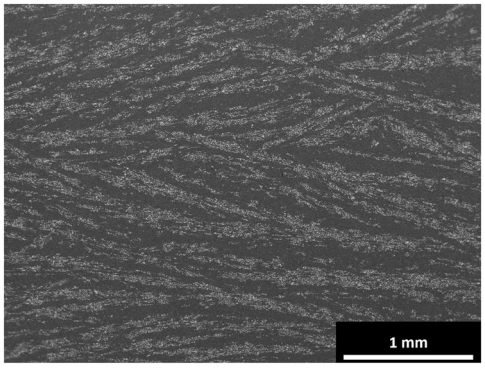

Fig. 11. SEM image of the SiC-C preforms with 5 % TIMREX KS25 graphite powder, showing the off-eutectic solidification of Si-8 at. pct Zr alloy in the SiC/C preforms with low C content.

The experimental results obtained in the reactive flow of the Si-Zr alloy in a micron-sized single capillary channel of glassy carbon are presented in our previous work [24]. We observed that increasing the infiltration temperature to 1700 °C might increase the infiltration depth. The increased length of infiltration is caused by the non-isothermal infiltration of the 10 μm glassy carbon microchannel. The result of the infiltration of the preform with TIMREX KS 25 powder of mass fractions from 20 % to 30 % and infiltrated at 1700 °C by the near-eutectic Si-Zr alloy showed, however, lower infiltration depth as compared to that of the similar preforms infiltrated at 1500 °C. This can also be confirmed by the lower density of the infiltrated preforms. The major differences between a single microchannel capillary and preform infiltration are the different tortuosity of the channel and the type of carbon. The carbon in the single microchannel experiment is glassy, yet the carbon and in the preform is graphitic. White et al. [26] and Voytovych et al. [27] have shown that the reaction rate of Si with C and the nature of the produced SiC are material-dependent. Secondly the tortuosity of the pore structure and the presence of pores with diameters lower than 10 μm hinder longer infiltration lengths obtained for non-isothermal infiltration over the peritectic temperature of the Si_2Zr formation.

Increasing the graphite particle size used to make the SiC-C preforms by changing the graphite powder from TIMREX KS 25 to TIMREX KS 44 resulted in preforms with a higher total porosity and modal pore size. The slightly higher porosity and modal pore size, as compared to preforms with TIMREX KS25 graphite powder, helps steering the infiltration closer to the core. However, the preform with a graphite mass fraction of 30% was still not completely infiltrated. A similar banding effect at the core can also be observed here. The measured densities after infiltration show that the preform with a mass fraction of 20 % TIMREX KS44 graphite powder produces discs with the highest density of 3.43 g/cm^3. However, it is worth noting that the bigger graphite particles of TIMREX KS44 graphite powder did not completely convert to SiC by reaction with Si from the alloy. From our previous study [28] of sessile drop experiments of Si and near-eutectic Si-Zr alloy on glassy carbon plates, we found that the maximum reaction layer of SiC formed on glassy carbon was around 5 μm for both pure Si and near-eutectic Si-Zr alloy. Additionally, Voytovych et al. [17], showed that the maximum reaction layer thickness on graphite is approximately 1520 μm. The liquid Si reacts with the C and forms a micron thick permeable layer of SiC, through which liquid Si can still diffuse through the pockets to rapidly form a thick layer of SiC until it reaches a threshold value of approximately 15–20 μm on graphite substrates and 10 μm on glassy carbon substrates. Further growth by grain-boundary diffusion of C is negligible

and only results in coarsening of the SiC grains rather than increasing the thickness of the SiC layer. The shape of the graphite particles is flaky and when one considers an isolated particle, the smaller dimension of the particle may be much smaller than 20 μm, however, during compaction and subsequent pyrolysis it is possible that some of the particles may agglomerate forming a cluster with dimensions exceeding the critical maximum thickness of the C particle. Although the preform with 20% TIMREXKS44 graphite powder is completely infiltrated with negligible porosity, the residual unreacted graphite may make it unsuitable for applications requiring high temperature oxidation resistance.

5. Conclusion

SiC/C preform infiltration with varying graphite mass fraction and particle size showed that increasing the porosity is not sufficient in obtaining fully dense composites without residual Si, porosity and unreacted C. The infiltration results were in line with the analytical model developed in our previous work [23] for an ideal porosity of the preforms with a given SiC/C ratio. The best conversion and densification were obtained for preforms made from SiC F800 and 15 % TIMREX KS 25 graphite powder, having an initial preform porosity of 33 % as measured by MIP. The infiltrated sample had less than 1 % of residual porosity and graphite with SiC being the predominant phase, Si_2Zr and minimal residual Si.

Precipitation of the solid Zr silicides at the infiltration front was the major cause of pore blocking in the case of the carbonaceous preforms infiltrated by Si- 8 at. pct Zr alloy, unlike the formation of SiC in the case of infiltration by pure Si. Increasing the processing temperature above the peritectic temperature did not enable higher infiltration, as suggested by the differential non-isothermal model developed for the infiltration length of the alloy in a micro-channel. Preforms with pore sizes lower than 10 μm and irregular pore structures resulted in faster pore clogging at higher temperatures, as suggested by the isothermal model[23].

Declaration of Competing Interest

The authors declare that they have no known competing financial interests or personal relationships that could have appeared to influence the work reported in this paper.

Acknowledgements

The authors are grateful to Swiss National Science Foundation (SNSF) for funding the project “Study and characterisation of silicon metal alloys systems for the reactive infiltration process of ceramic matrix composites” (Grant number 200021 163017).

Appendix A. Supporting information

Supplementary data associated with this article can be found in the online version at doi:10.1016/j.jeurceramsoc.2022.09.036.

References

[1] P. POPPER, Special ceramics, Soil Sci. 98 (1964) 142.
[2] G.S. Corman, K.L. Luthra, Silicon melt infiltrated ceramic composites (HiPerComp™), in: Narottam P. Bansal (Ed.), Handbook of Ceramic Composites, Springer, 2005, pp. 99–115.
[3] G. Bianchi, P. Vavassori, A. Ortona, G. Annino, S. Gianella, B. Vila, M. Nagliati, M. Mallah, M. Valle, M. Orlandi, Reactive silicon infiltration of carbon-based preforms embedded in powder field modifiers heated by microwaves, Euromat (2015) (2015).
[4] W. Krenkel, F. Berndt, C/C–SiC composites for space applications and advanced friction systems, Mater. Sci. Eng. A 412 (2005) 177–181.
[5] W. Krenkel, B. Heidenreich, R. Renz, C/C-SiC composites for advanced friction systems, Adv. Eng. Mater. 4 (2002) 427–436.
[6] N.R. Calderon, M. Martinez-Escandell, J. Narciso, F. Rodriguez-Reinoso, Manufacture of biomorphic SiC components with homogeneous properties from sawdust by reactive infiltration with liquid silicon, J. Am. Ceram. Soc. 93 (2010) 1003–1009, https://doi.org/10.1111/j.1551-2916.2009.03572.x.
[7] H. Carpentier, O. Caty, Y. Le Petitcorps, E. Maire, A. Marchais, N. Eberling-Fux, G. Couégnat, In situ observation of the capillary infiltration of molten silicon in a SiC/SiC composite by X-ray radiography, J. Eur. Ceram. Soc. 42 (2022) 1947–1954, https://doi.org/10.1016/J.JEURCERAMSOC.2021.12.041.
[8] J. Roger, M. Avenel, L. Lapuyade, Characterization of SiC ceramics with complex porosity by capillary infiltration: Part B – filling by molten silicon at 1500 °C, J. Eur. Ceram. Soc. 40 (2020) 1869–1876, https://doi.org/10.1016/J.JEURCERAMSOC.2019.12.050.
[9] R.P. Messner, Y. Chiang, Liquid-phase reaction-bonding of silicon carbide using alloyed silicon-molybdenum melts, J. Am. Ceram. Soc. 73 (1990) 1193–1200.
[10] O. Chakrabarti, P.K. Das, Reactive infiltration of Si-Mo alloyed melt into carbonaceous preforms of silicon carbide, J. Am. Ceram. Soc. 83 (2000) 1548–1550.
[11] T. Tsunoura, Y. Okubo, K. Yoshida, T. Yano, T. Aoki, T. Ogasawara, Oxidation behavior of monolithic HfSi2 and SiC fiber-reinforced composites fabricated by melt infiltration using Si–8.5 at% Hf alloy at 800–1200°C in dry air, J. Ceram. Soc. Jpn. 126 (2018) 27–33.
[12] R.B. Reitz, F.W. Zok, C.G. Levi, Reactive alloy melt infiltration for SiC composite matrices: mechanistic insights, J. Am. Ceram. Soc. 100 (2017) 5471–5481.
[13] T. Tsunoura, K. Yoshida, T. Yano, T. Aoki, T. Ogasawara, Fabrication and bending behavior of amorphous SiC-fiber-reinforced Si-Co eutectic alloy composites at elevated temperatures, Compos. Part B Eng. 164 (2019) 769–777.
[14] T. Aoki, T. Ogasawara, Y. Okubo, K. Yoshida, T. Yano, Fabrication and properties of Si− Hf alloy melt-infiltrated Tyranno ZMI fiber/SiC-based matrix composites, Compos. Part A Appl. Sci. Manuf. 66 (2014) 155–162.
[15] M. Caccia, S. Amore, D. Giuranno, R. Novakovic, E. Ricci, J. Narciso, Towards optimization of SiC/CoSi2 composite material manufacture via reactive infiltration: wetting study of Si–Co alloys on carbon materials, J. Eur. Ceram. Soc. 35 (2015) 4099–4106, https://doi.org/10.1016/j.jeurceramsoc.2015.07.016.
[16] D. Giuranno, A. Polkowska, W. Polkowski, R. Novakovic, Wetting behavior and reactivity of liquid Si-10Zr alloy in contact with glassy carbon, J. Alloy. Compd. 822 (2020), 153643, https://doi.org/10.1016/J.JALLCOM.2020.153643.
[17] D. Giuranno, G. Bruzda, A. Polkowska, R. Nowak, W. Polkowski, A. Kudyba, N. Sobczak, F. Mocellin, R. Novakovic, Design of refractory SiC/ZrSi2 composites: wettability and spreading behavior of liquid Si-10Zr alloy in contact with SiC at high temperatures, J. Eur. Ceram. Soc. 40 (2020) 953–960, https://doi.org/10.1016/J.JEURCERAMSOC.2019.12.027.
[18] A.D. Camarano, D. Giuranno, J. Narciso, New advanced SiC-based composite materials for use in highly oxidizing environments: synthesis of SiC/IrSi3, J. Eur. Ceram. Soc. 40 (2020) 603–611, https://doi.org/10.1016/J.JEURCERAMSOC.2019.10.018.
[19] A. Camarano, M. Caccia, J.M. Molina, J. Narciso, Effects of Fe addition on the mechanical and thermo-mechanical properties of SiC/FeSi2/Si composites produced via reactive infiltration, Ceram. Int. 42 (2016) 10726–10733, https://doi.org/10.1016/J.CERAMINT.2016.03.196.
[20] S. Kimura, K. Terashima, A review of measurement of thermophysical properties of silicon melt, J. Cryst. Growth 180 (1997) 323–333.
[21] M. Aronovici, G. Bianchi, L. Ferrari, M. Barbato, S. Gianella, G. Scocchi, A. Ortona, Heat and mass transfer in ceramic lattices during high-temperature oxidation, J. Am. Ceram. Soc. 98 (2015) 2625–2633, https://doi.org/10.1111/jace.13658.
[22] N. Eustathopoulos, B. Drevet, Surface tension of liquid silicon: high or low value? J. Cryst. Growth 371 (2013) 77–83.
[23] M. Naikade, A. Ortona, T. Graule, L. Weber, Liquid metal infiltration of silicon based alloys into porous carbonaceous materials. Part I: modelling of channel filling and reaction phase formation, J. Eur. Ceram. Soc. 42 (2022) 1971–1983.
[24] M. Naikade, C. Hain, K. Kastelik, R. Brönnimann, G. Bianchi, A. Ortona, T. Graule, L. Weber, Liquid metal infiltration of silicon based alloys into porous carbonaceous materials. Part II: experimental verification of modelling approaches by infiltration of Si-Zr alloy into idealized microchannels, J. Eur. Ceram. Soc. 42 (2022) 1984–1994.
[25] J.M. Molina, R. Arpón, R.A. Saravanan, C. Garcıa-Cordovilla, E. Louis, J. Narciso, Threshold pressure for infiltration and particle specific surface area of particle compacts with bimodal size distributions, Scr. Mater. 51 (2004) 623–627.
[26] J.F. White, L. Ma, K. Forwald, D. Sichen, Reactions between silicon and graphite substrates at high temperature: in situ observations, Metall. Mater. Trans. B. 45 (2014) 150–160.
[27] R. Voytovych, R. Israel, N. Calderon, F. Hodaj, N. Eustathopoulos, Reactivity between liquid Si or Si alloys and graphite, J. Eur. Ceram. Soc. 32 (2012) 3825–3835.
[28] M. Naikade, B. Fankhänel, L. Weber, A. Ortona, M. Stelter, T. Graule, Studying the wettability of Si and eutectic Si-Zr alloy on carbon and silicon carbide by sessile drop experiments, J. Eur. Ceram. Soc. 39 (2019) 735–742, https://doi.org/10.1016/j.jeurceramsoc.2018.11.049.